Macromolecules
ARTICLE

Macromolecules **2009**, *42*, 8521–8533 **8521**
DOI: 10.1021/ma901478d

Oxygen Sorption in Glassy Polymers Studied at the Molecular Level

Sylvie Neyertz* and David Brown

LMOPS-UMR CNRS 5041, University of Savoie, Bât IUT, 73376 Le Bourget du Lac, Cedex, France

Received July 8, 2009

ABSTRACT: In glassy polymer membranes, experimental sorption isotherms for light gases are usually found to be concave to the pressure axis. In the present work, oxygen (O_2) transport through a fully atomistic polyimide membrane has been studied using large-scale molecular dynamics (MD) simulations under five different conditions of applied external gas pressure. The concave behavior is well reproduced by the model and the initial gas uptake is linked to two distinct mobility modes. Because of a strong chemical potential gradient, the penetrants first undergo a rapid adsorption at the polymer surface at the very start of the simulations, which results in a complete saturation of the interfacial region. The average gas concentration at the interface then hardly changes with time and a quasi dynamic equilibrium is established with the gas phase. This is followed by a second slower and diffusion-limited uptake mode, with the diffusion coefficient for the penetrant in the membrane being independent of the applied external pressure. Results are analyzed and discussed in order to provide a molecular foundation to the sorption isotherms. Although the uptake vs pressure curves are well described by the popular dual-mode (DMS) sorption model, there is no evidence of two different populations of sorbed species at the molecular level. Boltzmann weighted probability densities of test-particle insertion energies are found to be described by single Gaussian distributions, thus supporting the site-distribution (SD) model.

1. Introduction

Transport of gases in dense polymer membranes typically rely on a sorption−diffusion mechanism: gas molecules in an upstream compartment enter the polymer matrix, diffuse across it, and finally desorb on a downstream gas compartment.[1] Many polymers are able to provide preferential transport for specific molecular species while acting as a barrier against others, a property which is at the basis of gas-separation applications.[2] In the case of glassy polymers, sorption isotherms with respect to small low-solubility penetrants are found to be concave to the pressure axis. They are most often fitted to the so-called empirical "dual-mode" (DMS) sorption model,[3−5] which combines both Henry's law and Langmuir mode sorptions, but other formalisms such as, e.g., the site-distribution (SD) model have been proposed to describe sorption in these systems.[6,7] The polyimide family, where the choice of the basic chemical motifs associated with various membrane processing parameters can lead to good transport properties with respect to oxygen, nitrogen, carbon dioxide or methane, is known to exhibit the concave uptake vs pressure behavior for the low-solubility penetrants.[2,8−19]

While gas permeation in polyimides has been considerably studied from an experimental point-of-view,[2,8] there are still in comparison fairly few molecular dynamics (MD) simulations[20] in the literature, with the model densities being in very close agreement (≤1−2%) with experimental values.[21−26] A fully atomistic and complex representation is required for glassy polyimides, the computationally expensive electrostatic interactions cannot be ignored and specific techniques, such as hybrid pivot Monte Carlo−molecular dynamics (PMC−MD) single-chain sampling, have to be used to create the starting configurations.[21,24−28] Another difficulty is linked to the creation of actual surfaces in the polymer, if a true membrane model is to be preferred to a bulk model. The most common approach is that of extending one simulation box axis in order to eliminate interactions of the parent chains with their images in that direction,[29−35] but this requires significant mobility of the polymer in order to relax from bulk to surface-like chains. In our experience, the density of the polyimide quickly decreases in the extended direction and the model is too rigid to be able to redensify under the MD time-scale. It is also possible to use multiscale approaches,[32,36−43] but well-parametrized coarse-grained models at the right temperatures have to be built and intricate reverse mapping procedures have to be used. It is thus not surprising that most of the polyimide+gas MD models available are bulk simulations (see e.g. refs 22−25, 44, and 45) and thus cannot possibly assess any "skin-effects".

We have recently designed a procedure loosely based on the experimental solvent-casting process for creating fully atomistic 40-mers ODPA−ODA polyimide (Figure 1) membrane models.[24,46−48]

Among those, a free-standing ODPA−ODA membrane of width ∼60 Å (i.e., ∼50 000 atoms) associated with gas reservoirs of 3500 O_2 molecules on either side was used to model oxygen transport.[48] Such dimensions for the polymer remain relatively small with respect to experimental thicknesses of a few micrometers,[49] but they are already about 10 times larger than the typical MD boxes used for fully atomistic bulk glassy systems.[22,23,25] Oxygen adsorption, penetration and diffusion through the ODPA−ODA membrane was followed over a total of 13000 ps, which turned out to be computationally very expensive, mostly because of the electrostatic interactions required to maintain the cohesion of the membrane.[48] In the aforementioned simulation, the reservoir size had been chosen in an attempt to have enough O_2 going into and diffusing through the membrane within the available MD production run. This corresponded to a pressure of $P \sim 270$ bar and was obviously much larger than the pressure range used experimentally, i.e., typically ∼2−3 bar for O_2.[49]

*Corresponding authors. E-mail: Sylvie.Neyertz@univ-savoie.fr.

Published on Web 08/28/2009

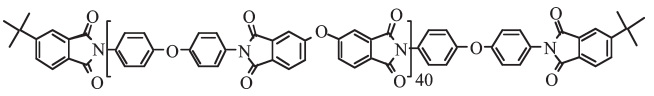

Figure 1. ODPA−ODA polyimide chain.

While it is clear that a compromise has to be found between the applied pressure and sufficient statistics to characterize diffusion in MD simulations, we are not aware of any systematic study of the effect of external pressure on oxygen transport in such glassy polymer membrane models. As such, we have repeated the calculation with different reservoir sizes: 100-molecules ($P \sim 4$ bar), 250-molecules ($P \sim 10$ bar), 500-molecules ($P \sim 23$ bar) and 1750-molecules ($P \sim 110$ bar) to be compared to the 3500-molecules ($P \sim 270$ bar) results.[48] In addition to modeling considerations, we also wanted to assess whether such models could reproduce a similar behavior to that seen in experiment as a function of pressure. As will be shown, the sorption curve is indeed concave with respect to the pressure. This study thus provides a molecular picture of the early stages of sorption in glassy polymers.

The characteristics of the polyimide membrane model are briefly summarized in section 2. The insertion procedure for O_2 and the corresponding pressures are described in section 3. The O_2 permeation parameters for the polyimide membrane are characterized and discussed with respect to the gas external pressure in section 4. All calculations were performed using the MD code of the *gmq* package[50] in its parallel form on the French IDRIS, CINES, and CCRT supercomputing centers as well as on the MUST Linux server at the University of Savoie.

2. The Polyimide Model Membrane

The preparation procedure for the ODPA−ODA polymer has already been described in detail[24,46−48] and so only the main features of the 49800-atom free-standing membrane[48] will be summarized here. Each of the 24 ODPA−ODA chains (Figure 1) has a length of 40 monomers and 2075 atoms. The force-field for the polyimide is the same as described before.[21,25] Bonds are kept rigid and the integration time-step is 10^{-15} s. The "bonded" interactions arising from near-neighbor connections in a chain include angle-bending, torsional and out-of-plane interactions. The "nonbonded" excluded-volume Lennard-Jones (LJ) 12−6 and electrostatic potentials are applied to all atom pairs separated by more than two bonds on the same chain or belonging to different chains. Standard Lorentz−Berthelot combination rules[20] are used for all cross-terms and long-range electrostatic energies are evaluated using the Ewald summation method.[51,52]

The preparation procedure for the polyimide membrane[24,46−48] is loosely based on the experimental solvent-casting process,[49,53] which involves preparing a solution of the polymer in, e.g., *m*-cresol and casting it onto a glass plate. Solvent is subsequently removed through an appropriate heat treatment and the film is peeled off the glass plate. The solvation procedure was mimicked here by randomly distributing 24 PMC−MD single-chain sampled[24] molecules in a simulation box with the density of an ideal (90% *m*-cresol/10% ODPA−ODA) solution. Since solvent evaporation occurs mostly through the uppermost surface of a film, the basis vectors in the x and y direction were left at the value expected from the experimental ODPA−ODA density $\rho_{exp} = 1368$ kg m^{-3},[54] while the basis vector in the z direction was increased. The full potential was progressively introduced and an impenetrable wall subsequently added on either side of the "solvated" polymer. The process of densification resulting from solvent evaporation was modeled by compressing in an affine manner the wall + polymer system in the z direction until ρ_{exp} was reached at the center-of-mass (COM) of the confined membrane. The wall compression has also been used by Kikuchi et al.,[55,56] for a bulk polyisoprene chain by starting from a box big enough to contain a single chain under the periodic boundary conditions. Following high-temperature relaxation and cooling down of the system, the wall was pushed away in order to avoid any interactions with the polymer while preventing gas probes from escaping into the vacuum. Once free to move, the polymer chains relaxed slightly in the z-direction to lead to a membrane width of ∼60 Å in a total box of $112 \times 113 \times 130$ Å^3. The Ewald sum was found to converge[51,52] using $\alpha = 0.15$ Å^{-1} and $K_{max} = 13$, and a real-space truncation of 10 Å. The excluded-volume potentials were also truncated at 10 Å. The temperature T was maintained at 300 K through loose-coupling to a heat bath[57] with a coupling constant of 0.1 ps.

As noted before,[24,46−48] some questions remain open with respect to the preparation procedure. It would clearly have been preferable to dissolve the polymer in an explicit solvent and subsequently evaporate the solvent, as has been reported for coarse-grained bead−spring models.[58,59] Unfortunately, adding explicit solvent molecules is simply too expensive in terms of computational resources, and in any case, it is highly unlikely that the rigid polyimide chains would be able to adapt to the ever-changing concentration within the MD time scale. Another consequence of the preparation procedure is that the combined effects of the relatively "small size" of the model with respect to experimental dimensions, the compression step and the very-low mobility lead to chains being actually more surface-like than bulk-like. This can be partially compensated by running separate bulk models which represent the membrane core.[48] In addition, it is important to point out that the features of our membrane[48] are in excellent agreement with those of the surface-layer chains reported for much shorter, more flexible and usually less-realistic polymers, in which the system sizes and relaxation times often allow for the gradual change from surface layers to bulk-like structure in the middle of the membrane models.[24,30−36,47,55,60−71] This indicates that our preparation technique gives at least reasonable configurations for the surface-layer chains of our polyimide.

The slab mass density distribution as a function of the distance along the z-axis to the 49800-atom polyimide COM, $\rho(z)$, was found to display the sigmoidal profile characteristic of free-standing interfaces. It could be fitted to the following hyperbolic equation:[72,73]

$$\rho(z) = \rho_{middle}\frac{1-\tanh[2(z-h)/w]}{2} \qquad (1)$$

with $\rho_{middle} = 1325$ kg m^{-3} being the density in the middle region of the film, $h = 23.2$ Å the location of the interface with respect to the membrane COM and $w = 4.6$ Å the interfacial width. The fact that the middle region density ρ_{middle} is ∼3% lower than the experimental bulk value of 1368 kg m^{-3},[54] can be linked to the chain configurations. Indeed, chains at the vicinity of an interface are known to align in a parallel fashion with respect to the surface and to adopt a "pancake"-like nearly two-dimensional structure.[74−79] In this specific case, the alignment and flattening persist, albeit quite attenuated, into the core of the model, a fact which is obviously related to the preparation procedure as noted above.[24,46,47] As can be expected from glassy membranes, the polymer mean-square displacements (MSD) are very small, with a slight increase at the vicinity of the interfaces. This allowed us to define a "dynamical interfacial thickness" of ∼15−20 Å from its gas reservoir, which is quite a bit larger than the "structural interfacial thickness" w obtained from the mass density (eq 1). Some close-ups of the polymer interfaces are shown in Figure 2. It is clear that the definitions of the thickness for the interface and the "boundaries" of a

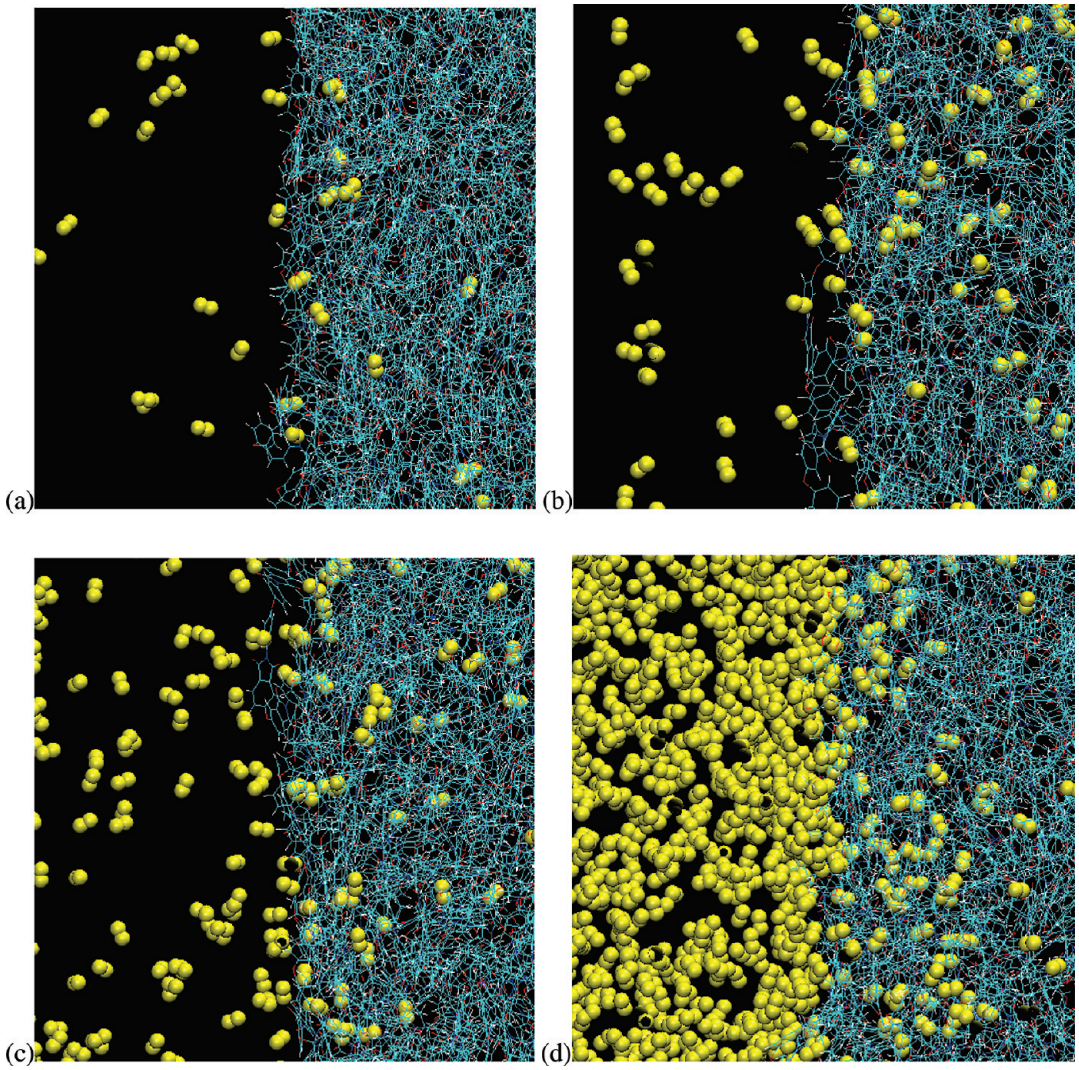

Figure 2. Snapshots at 13000 ps displaying the polymer membrane in a wire-frame and the O_2 penetrants in space-filling models. The color code is the following: cyan = polyimide C, red = polyimide O, blue = polyimide N, white = polyimide H, and yellow = penetrant O. These schematic representations are displayed using the VMD 1.8.2 software.[90] The different reservoir pressures shown are (a) $P = 4$ bar, (b) $P = 10$ bar, (c) $P = 23$ bar, and (d) $P = 270$ bar.

free-standing membrane are very subjective in the case of such rough surfaces, since they depend both on the property considered and on the way it is analyzed. It should also be noted that, while the chains are indeed aligned and flattened, they are actually intertwined and there is no sign of layers.

3. The Model Penetrant Gas

The penetrant parameters were taken from the two-center Fisher−Lago potential for pure oxygen.[80] Equal numbers of gas molecules were inserted into the empty spaces between the membrane and the impenetrable wall at the start of each simulation. Results from both sides of the membrane were used to improve the statistics, as the actual numbers of exchanges of gas molecules between the two reservoirs are negligible within the simulation time scale.[48] In the model, the O_2 molecules interact with each other as well as with the polymer. We had noted previously that removing $O_2\cdots O_2$ interactions results in an artifact where the adsorption layer at the interface takes on unphysical proportions. As such the gas−gas interaction parameters in our simulations were not artificially set to zero.

For bulk polymer models and small penetrants that do not swell a matrix, it is possible to estimate relatively easily the amount of gas to insert into the polymer for a given external gas pressure.[24,48] Unfortunately, this is not the case for a true membrane model. The amount of gas which will adsorb onto the membrane is *a priori* unknown and its entry into the dense matrix will depend on the rate of diffusion, which is slow for gas in polyimides in comparison to the MD time scale.[2] In such simulations, we are then faced with the problem of having enough penetrants going into and diffusing through the membrane within the production run so that the results are statistically significant. In order to assess the behavior of the oxygen model with respect to that of an ideal gas, a series of constant-volume and temperature (*NVT*) simulations of pure 1000-molecule O_2 systems were carried out at 300 K in the 5−500 kg m^{-3} oxygen density range and the associated pressures P were recorded. It was found that all P were very close to those estimated from $PV = nk_BT$ with k_B being the Boltzmann constant, V the volume, and n the number of O_2 molecules, providing that the oxygen density was under 380 kg m^{-3}. It was then initially decided to use a value close to the upper limit of the interval, i.e., ∼350 kg m^{-3} and $P \sim 270$ bar. This meant inserting 3500 O_2 molecule *per* reservoir.[48]

The evaluation of the actual gas pressure in the reservoirs is made complicated by the roughness of the polyimide surfaces (see Figure 2) and by the accumulation of O_2 at such interfaces. Two different approaches were used. The first one required the

probability of insertion of a gas molecule into the system, p_{ip}, which was obtained from a test-particle insertion (TPI) method.[81] In the TPI method, a probe gas molecule is repeatedly inserted at random positions in the MD box and the changes in potential energy associated with the virtual insertion, $\Delta\Phi$, are used to obtain the average Boltzmann factor using the following equation:

$$S \approx p_{ip} = \left\langle \exp\left(-\frac{\Delta\Phi}{k_B T}\right)\right\rangle \quad (2)$$

which is known to give a good approximation of the solubility, S, for small penetrants such as oxygen.[82] The probabilities of insertion of an O_2 into the system can be averaged over all configurations of the production run, thus leading to $\langle p_{ip}\rangle$, which can be further resolved as a function of z for a slab of given width $\langle p_{ip}(z)\rangle$. p_{ip} is also related to the excess chemical potential of the gas in the polymer, μ_{ex} by

$$\mu_{ex} = -k_B T \ln\left\langle \exp\left(-\frac{\Delta\Phi}{k_B T}\right)\right\rangle = -k_B T \ln(p_{ip}) \quad (3)$$

from which we can obtain $\langle \mu_{ex}\rangle$, which can itself then be resolved as a function of z, $\langle \mu_{ex}(z)\rangle$. For the evaluation of the pressure, the average reservoir gas density was measured in the part of the box where $\langle p_{ip}(z)\rangle \approx 1$ and thus $\langle \mu_{ex}(z)\rangle \approx 0$; i.e., the penetrant can be considered as being in an ideal gas phase.

A second approach used a direct measurement of the P_{zz} component of the pressure tensor from the atomic momentum flux[83] across virtual interfaces placed perpendicular to the z direction in the gas reservoirs. The values of P_{zz} obtained in that way were very similar to those of the indirect approach and confirmed the quasi-ideality of the gas in the center of the reservoirs.

The initial model $P \sim 270$ bar reservoir was about 100 times larger than the typical pressures used experimentally for O_2, i.e. between ~2−3 bar[49,84] up to ~10 bar.[85−87] In the latter case, the pressure is reported as having little influence on the permeability.[2,85,86,88,89] However, while $P \sim 270$ bar can be easily justified from a simulation point-of-view, it is clear that its influence on the model results should be checked. As such, different reservoir sizes were considered: 100 molecules, 250 molecules, 500 molecules, and 1750 molecules. The average densities in the middle of those reservoirs were about ~5, 14, 31, and 143 kg m^{-3}, respectively. The average pressures P could thus be estimated at ~4 bar (100 O_2), ~10 bar (250 O_2), ~23 bar (500 O_2), and ~110 bar (1750 O_2). All simulations were carried out over 13000 ps so as to compare their results with the 3500 molecule reservoir under the same conditions. Configurations were stored at 10 ps intervals, and thermodynamic and conformational data every 1 ps for postanalysis. A series of short 100 ps simulations was carried out in parallel with the configurations being stored at 1 ps intervals in order to better characterize the initial adsorption phase.

4. Permeation as a Function of Oxygen Pressure

The main purpose of this work is to study oxygen transport through our fully atomistic ODPA−ODA membrane as a function of the reservoir pressure. It should be noted that no specific swelling effect that could be separated from the natural fluctuations of the glassy matrix were observed in any of the systems. As found experimentally for O_2,[2] there is no plasticization effect in these simulations.

4.1. Oxygen Trajectories. Trajectories of individual oxygen molecules within the membrane can be described as a combination of oscillations within available voids in the polymer and occasional jumps between different voids upon opening of temporary channels, which agrees with the typical behavior for small penetrants in glassy dense matrices.[82,91,92] Only very few molecules manage to cross the membrane within the 13 ns MD time scale (less than 0.2% for the higher P and none for the smaller P), but shorter paths exhibit the same types of trajectories as longer ones. Figure 3 displays the complexity of such an O_2 motion in the $P = 110$ bar system.

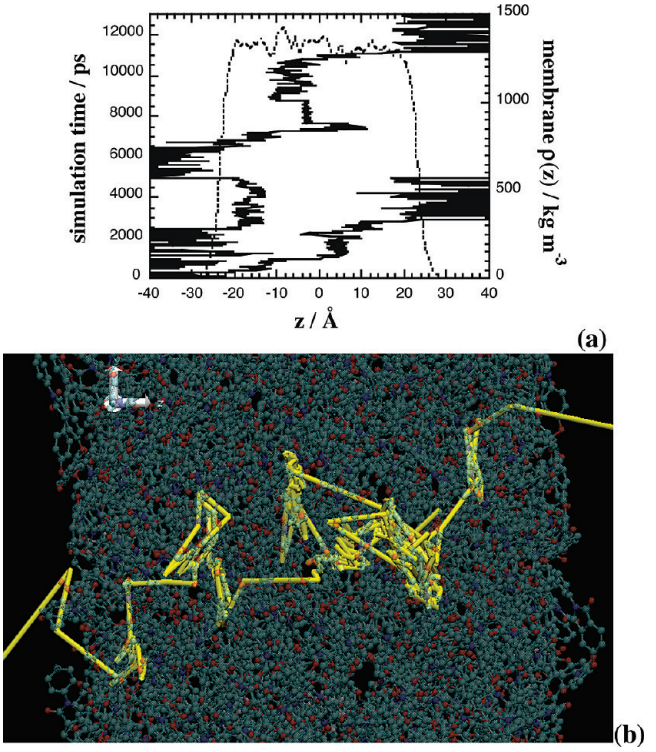

Figure 3. (a) Trajectories along the z direction for two different O_2 molecules crossing the membrane in the $P = 110$ bar system (lines). Also shown is the average polymer mass density as a function of z (short dash) evaluated with a slab width of 1 Å. (b) A schematic representation (yellow thick line) of an O_2 trajectory displayed using VMD 1.8.2. Note that configurations have been accumulated every 10 ps so that every segment actually spans that time-interval. The polymer matrix at 13 ns is displayed in the background with the "transparent" option of the visualization package (same color code as Figure 2).

The rapid oscillations in the gas phase are damped in the polymer matrix, but it is clear from Figure 3 that the paths are far from being identical. Some caution is necessary concerning the schematic O_2 trajectory in Figure 3b as MD configurations have been accumulated every 10 ps and some individual jump events can occur on a shorter time scale. It should thus be seen as a global illustration of the path taken by that specific molecule. Although the general pattern of oscillations within voids and jumps is always present, individual analyses show that there are actually about as many different trajectories as penetrants. The jumps and times-of-residence depend on the location and the local mobility of the matrix, some jumps are productive in terms of diffusion while others are not, and the penetrant can get stuck or even come back to the region it has just left. However, mobility tends to be quite smooth and we do not find any evidence of clustering within the membrane, except for the concentration at the interface (see later). As noted in the $P = 270$ bar work,[48] the penetrants can also move in the x- or y-direction on similar length scales. This suggests that they are subject to the same topological constraints than in the z-direction and

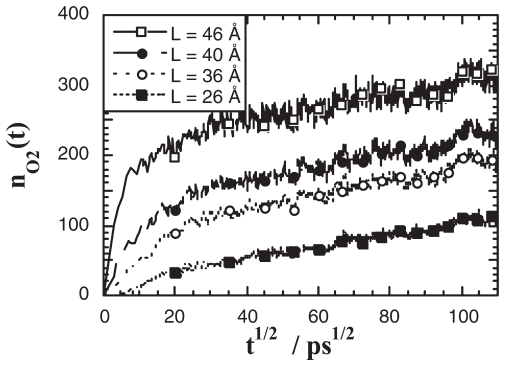

Figure 4. Total number of oxygen molecules $n_{O_2}(t)$ entering the membrane as a function of the square root of time in the $P = 23$ bar system. Because of the uncertainty in the definition of the membrane thickness, L, several values related to the interface have been considered.

that their motion is primarily linked to very local features in the matrix. Flattened chain configurations thus do not really appear to make any difference. As such, and within the available statistical resolution, no real anisotropy in the core of the membrane could be detected either in the x-, y-, or z-directions.

4.2. Gas Uptake Curves. The main difficulty in following O_2 uptake curves is a clear definition of the width of the membrane L. As seen in Figure 2, model glassy polymer surfaces are quite rough. This is actually also the case in experimental permeation measurements, where the main source of error lies in the determination of the membrane thickness.[93] Analyses were thus carried out using several possible definitions for the thickness:[48] $L = 46$ Å, which comes from the hyperbolic fit to the mass density, $L = 40$ Å, which was deemed as being the boundary for the slowest gas diffusion mode, $L = 36$ Å, which corresponds to the start of the dense part of the membrane, and $L = 26$ Å, which is situated well inside the membrane at the inner limit of its dynamical interface. Figure 4 displays the total number of O_2 molecules, $n_{O_2}(t)$, entering the membrane (from both reservoirs) for these various definitions of the membrane width as a function of the square root of time, $t^{1/2}$, for the $P = 23$ bar system.

Trends in the uptake curves for the other systems under study are similar to those in Figure 4, although $n_{O_2}(t)$ changes with pressure and statistics are obviously less good for the lower pressure systems. The initial jump seen for $L = 46$, 40, and 36 Å is characteristic of a very fast gas adsorption phase, which occurs before 250 ps and for most of it before 50 ps. This is an irreversible process, but close examinations of the trajectories show that there are continuous exchanges between nonadsorbed gas molecules in the reservoir and those adsorbed at the polymer surface. Defining L as being 46 or 40 Å corresponds to the low-density parts of the polymer, where the penetrants infiltrate easily. However, it is interesting to note that an attenuated jump is still present in the $L = 36$ Å curve of Figure 4. It only really disappears for $L = 26$ Å, which has been defined, from the polymer mean-square displacements, as being the "dynamical interfacial thickness" of our ODPA−ODA membrane,[48] that is the region where the MSDs of polymer atoms come back to their inner core value. The fact that dynamical properties are affected in the vicinity of an interface on a larger range than structural properties is well-known,[94] and is attributed to the transmission of mobility due to the molecular connectivity.[61] The difference between $L = 36$ Å and $L = 26$ Å shows that the penetrant is able to get rapidly up to the dynamical interface. In all cases, after the initial adsorption phase, a slower rate of

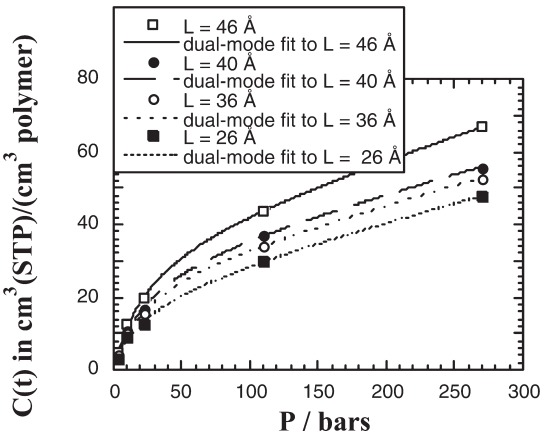

Figure 5. Gas concentration $C(t)$ in the membrane at $t = 13000$ ps as a function of reservoir pressure P and membrane thickness L. Data issued directly from the simulations are displayed with symbols. The lines are fits of the data to the dual-mode sorption isotherm model (eq 5).

uptake and a more linear dependence with respect to $t^{1/2}$ then takes over with a similar slope regardless of the definition of L. It is often assumed that a linear relationship between the weight gain of the polymer and $t^{1/2}$ is the signature of Fickian diffusion.[95,96] However, the $n_{O_2}(t)$ curves are also found to be quasi-linear with respect to t^{α} ($0 < \alpha \leq 1$), and thus we cannot unambiguously characterize the diffusion regime in that way. The representation of the uptake curves vs $t^{1/2}$ is preferred here as the initial adsorption phase is well discriminated from the rest of the diffusive behavior.

The concentrations of O_2 molecules in the membrane were also analyzed as a function of the reservoir pressure. The penetrant concentration at time t, $C(t)$, is the total number of molecules in the membrane $n_{O_2}(t)$ divided by the volume of the polymer V_{pol} at time t. The volume V_g occupied by the gas at temperature T and pressure P under the ideal gas approximation is

$$V_g = \frac{n_{O_2}(t) k_B T}{P} \tag{4a}$$

The same can be written for the specific standard temperature and pressure (STP: 273.15 K; 1.013×10^5 Pa) conditions:

$$V_g^{STP} = \frac{n_{O_2}(t) k_B T^{STP}}{P^{STP}} \tag{4b}$$

which leads to the following expression between $C(t)$ expressed in cm^3(STP)/(cm^3 polymer) and $n_{O_2}(t)$:

$$C(t) = \frac{V_g^{STP}}{V_{pol}} = \frac{n_{O_2}(t) k_B T^{STP}}{P^{STP} V_{pol}} \tag{4c}$$

The $C(t)$ results are displayed in Figure 5 for $t = 13000$ ps taking into account the various possible definitions of the membrane thickness.

The $C(t)$ are concave to the pressure axis, which is in agreement with the experimental behavior for such glassy polymers. Similar curves are obtained if t is less than 13000 ps, albeit with lower $C(t)$. In the vast experimental literature on the subject (for a review, see e.g. ref 2), such data are most often described by the "dual-mode" (DMS) sorption model shown in eq 5[3]

$$C(t) = C_D + C_H = k_D P + C_H' \frac{bP}{(1+bP)} \tag{5}$$

Table 1. Dual-Mode Sorption Model Parameters k_D, C'_H, and b Obtained by Fitting the $C(t)$ Data at t = 13000 ps in Figure 5 to the Form of Eq 5[a]

L (Å)	k_D (cm^3(STP) cm^{-3} bar^{-1})	C'_H (cm^3(STP) cm^{-3})	b (bar^{-1})
46	0.12	38	0.04
40	0.10	32	0.04
36	0.10	28	0.04
26	0.10	23	0.04

[a] L is the width considered for the membrane.

where the subscript D refers to Henry's law mode sorption and the subscript H to Langmuir mode sorption. In the DMS model, k_D is Henry's law solubility coefficient and is interpreted as characterizing sorption into the densified equilibrium matrix of the glassy polymer. Langmuir sorption is thought to be related to the nonequilibrium excess volume associated with the glassy state and is described by two parameters, the Langmuir sorption capacity C'_H and the Langmuir affinity parameter b. Although the DMS model is able to correlate with various factors such as the glass transition temperature (T_g), fractional free volume or gas transport parameters, it should be noted that statistical correlation analyses of experimentally reported parameters result in significant scatter.[5] Furthermore, careful analyses of experimental data obtained over increasing pressure ranges also show clearly that the adjustable parameters (k_D, C'_H and b) are not constant but vary systematically with the pressure range used.[4] In spite of the fact that the functional form of the DMS model gives reasonably good fits to experimental data, the parameters obtained in a specific range thus cannot really be considered as reliable predictors of what happens beyond the range of pressure fitted. These observations clearly undermine the physical basis of the DMS model but its simplicity has led to it remaining popular.

As seen in Figure 5 (lines), our simulated $C(t)$ do fit very well to the form of eq 5. The actual DMS coefficients are given in Table 1.

These parameters can not be compared directly to experimental data as our simulations are not in equilibrium and we are not aware of any experimentally derived DMS parameters for O_2 in ODPA−ODA. The only DMS parameter that depends on the definition of the membrane width L is the Langmuir sorption capacity C'_H. It is also the dominating term and suggests that the gas uptake here is very much of Langmuir origin, that is the penetrant sorbs into predefined adsorption sites.[97] This effect agrees with C'_H being interpreted as a measure of voids accessible to the penetrant. Experimentally, k_D and b are found to be often correlated with penetrant condensability,[98] which would agree with their values remaining constant in Table 1.

On the other hand, the assumption behind the DMS model that there would be two "populations" of sorbed species in local equilibrium with one another, i.e., those in long-lived nonequilibrium free-volume elements and those dissolved in more densely packed regions within the polymers,[2] is difficult to assess here. As seen in section 4.1, the individual trajectories of the penetrants are all different but they systematically exhibit some combination of long-lived oscillations-in-voids and jumps. This suggests that if there were two populations, each individual O_2 molecule would contribute at time t either to one or to the other depending on its position at that specific time. As such, the separate diffusion coefficients assigned to the two types of sorption sites, Henry's law D_D and Langmuir D_H in the partial immobilization model[99] are not really supported by molecular evidence. It should also be noted that, in spite of the popularity of the DMS formalism, several other models have been proposed to describe sorption in glassy polymers.[2] Some of them involve lattice theories,[100−102] which are also difficult to compare directly to a fully atomistic description. Another one is the site-distribution model introduced by Kirchheim,[6,7] which describes sorption in terms of a Gaussian distribution of site energies. This energy distribution is itself correlated to a volume distribution of the intermolecular space yielding different elastic distortion energies when occupied by solute molecules. We will give some supporting evidence for this model in the next section.

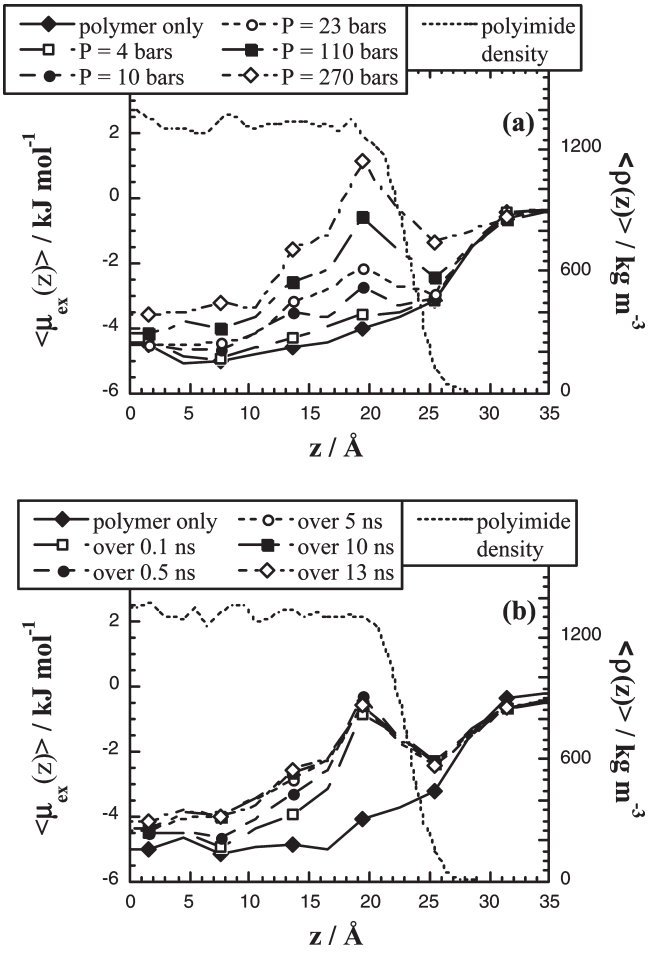

Figure 6. (a) Left axis: symmetrized $\langle\mu_{ex}(z)\rangle$ for O_2 in the ODPA−ODA membrane as a function of z accumulated over the full 13 ns production runs. Insertion energies were calculated by taking into account either the polymer matrix on its own in the P = 4 bar system (black diamonds) or the polymer matrix and all other O_2 penetrants for each gas reservoir pressure (other symbols). Right axis: polyimide average mass densities $\langle\rho(z)\rangle$ in the P = 4 bar system as a function of z. (b) Time dependence of $\langle\mu_{ex}(z)\rangle$ and polyimide average mass density $\langle\rho(z)\rangle$ in the P = 110 bar system. Analyses have been carried out from the start of the simulation over different time-intervals starting from 0.1 ns up to the full 13 ns production run.

4.3. Excess Chemical Potential. The average excess chemical potential $\langle\mu_{ex}\rangle$ of an O_2 probe into the ODPA−ODA membrane was resolved in the different systems as a function of z for slabs of width 3 Å (see eqs 2 and 3). Results for $\langle\mu_{ex}(z)\rangle$ are presented in Figure 6 for 40 million trials *per* system and a cutoff for van der Waals interactions equal to half the smallest box length (~56 Å). They were calculated taking into account either the polymer matrix on its own (black diamonds) or the polymer matrix and all other O_2 penetrants in each system under study (other symbols).

The $\langle \mu_{ex}(z) \rangle$ obtained for the free-standing membrane alone while ignoring its penetrants are very similar for all systems under study and the curves obtained from the $P = 4$ and $P = 110$ bar systems are displayed in Figure 6, parts a and b, respectively (black diamonds). This is consistent with the lack of matrix swelling and fairly little adjustment of the polymer structure to the penetrant. As found before, the solubility for O_2 is favored in the polymer membrane with respect to that in an isotropic bulk ($\langle \mu_{ex} \rangle = -2.3$ kJ mol^{-1} in a pure ODPA−ODA box).[23] This has been attributed both to the slightly lower density and to the specific configurations associated with surface chains.[48] Insertions in the denser parts of the membrane model ($|z| < 15$ Å) are most favorable as O_2 maximizes the number of attractive interactions with the polymer matrix. Those in the interfacial region only interact with the polymer on one side and the excess chemical potential tends, as expected, to zero as one gets further away from the membrane. This contributes to a gradient in the total chemical potential, which is the underlying driving force for diffusion (see section 4.4).[103−105] It is consistent with the very rapid adsorption of the gas onto the surface which systematically occurs at the start of the simulations for all reservoir sizes considered, up to the part where the solubility tends to level off.

The $\langle \mu_{ex}(z) \rangle$ can also be calculated with the other gas penetrants being taken into account in addition to the polymer matrix. Figure 6a displays the effect of reservoir pressure P and Figure 6b illustrates the time dependence of such analyses for $P = 110$ bar. The presence of penetrants in the membrane strongly affects the excess chemical potential, and hence the total chemical potential gradient. In all cases, $\langle \mu_{ex}(z) \rangle$ displays a peak around ∼20 Å from the COM, which becomes very pronounced when the pressure increases. Figure 6b shows that this peak is present at very short times and that its magnitude changes little afterward. It is clearly related to the aforementioned initial adsorption phase which leads to the voids in this region being quickly occupied. This pressure-dependent interface saturation phase lowers significantly the solubility of the penetrant in the interfacial region of the membrane and a quasi-equilibrium is quickly established with the gas phase. This is followed by a slower diffusion-limited mode as probes enter the inner parts of the matrix. As seen before for the $P = 270$ bar system[48] and as displayed in Figure 6b, the boundaries are at about ± 20 Å. This explains the progressive increase in $\langle \mu_{ex}(z) \rangle$ for $|z| < 20$ Å as the gradually increasing number of penetrants in the membrane lowers the solubility.

The $\langle \mu_{ex}(z) \rangle$ were also calculated while excluding the interactions with the polymer from the analyses but retaining those with the gas. These gas−gas $\langle \mu_{ex}(z) \rangle$ are not very favorable at the interface where the gas is concentrated and this is, as expected, pressure-dependent. However, they are almost equal to 0 within the dense part of the membrane, where there are relatively few gas molecules with respect to the sizes of the reservoirs. It further justifies the introduction of the gas on both sides of the model in order to improve statistics.

As for $\langle \mu_{ex} \rangle$, the changes in the potential energy associated with the virtual insertion of the O_2 probe in the test-particle insertion TPI method, $\Delta\Phi$ (see eq 2), can be resolved spatially as a function of z. Normalized probability density distributions for $\Delta\Phi/k_BT$, $\rho(\Delta\Phi/k_BT)$, were calculated for successive slabs of width 3 Å and were subsequently symmetrized over both sides of the membrane. The corresponding Boltzmann-factor weighted probability density distributions were obtained from the product of $\rho(\Delta\Phi/k_BT)$ with $\exp(-\Delta\Phi/k_BT)$ and are shown in Figure 7a for several slabs

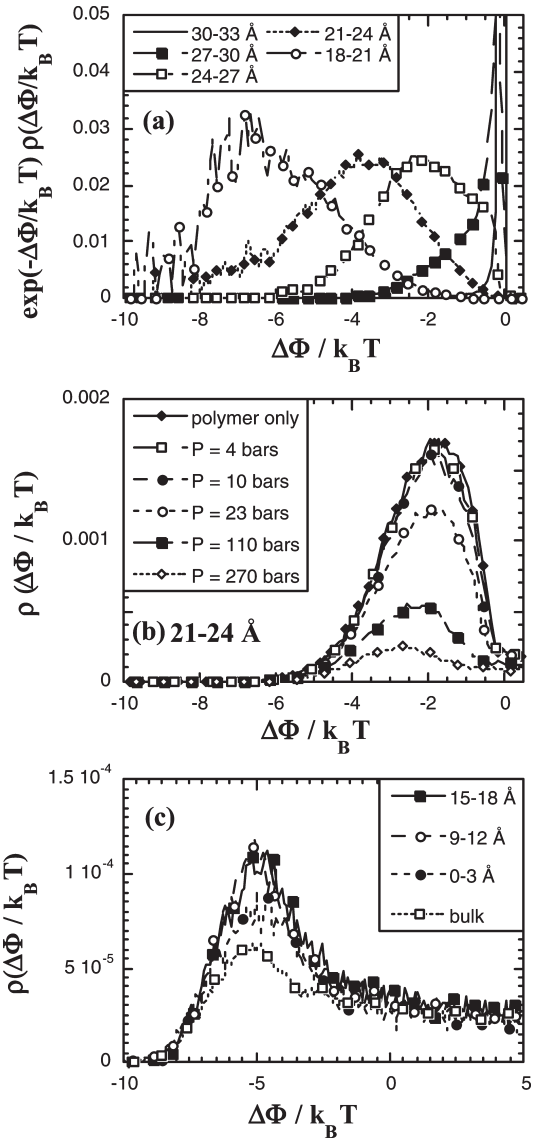

Figure 7. Symmetrized probability distributions associated with the changes in potential energy $\Delta\Phi$ upon repeated insertions of an O_2 probe. The $\rho(\Delta\Phi/k_BT)$ are resolved spatially in z for slabs of width 3 Å and for bins of size 0.1 in $\Delta\Phi/k_BT$. (a) Boltzmann-weighted $\rho(\Delta\Phi/k_BT)$ for slabs situated close to the structural interface for the pure polymer, (b) raw $\rho(\Delta\Phi/k_BT)$ for the 21−24 Å slab as a function of reservoir pressure, and (c) raw $\rho(\Delta\Phi/k_BT)$ for slabs situated in the dense part of the pure membrane compared to that in an isotropic bulk.

close to the structural interface of the pure membrane. The slab defined as $|z| = 30-33$ Å corresponds to that part of the reservoir next to the membrane, while $|z| = 27-30$ Å, $|z| = 24-27$ Å, $|z| = 21-24$ Å, and $|z| = 18-21$ Å can be associated with increasing densities at the polymer interface. As expected, there is a narrow peak close to zero for $\Delta\Phi$ in the gas phase. The Boltzmann-factor weighted probability density distributions then get wider and more displaced toward the left as z decreases. It is clearly due to the progressive increase in matrix density, which leads to more attractive interactions between the penetrant and the polymer, and consequently to more negative insertion energies and more favorable sites for probe insertions. As seen in Figure 7a, a drawback of the Boltzmann-weighted representation is that the exponential term, $\exp(-\Delta\Phi/k_BT)$, becomes very large as $\Delta\Phi$ gets more negative, and leads to small "peaks" which are basically artifacts of insufficient averaging.

As such, we rather chose to display the raw $\rho(\Delta\Phi/k_BT)$ data to illustrate the dependence of the probability density distribution on the reservoir pressure in Figure 7b, that is taking into account the other penetrants in the TPI analysis. The example shown is for the $|z| = 21-24$ Å slab which includes the location of the interface obtained from the hyperbolic definition ($h = 23.2$ Å from eq 1). The presence of other O_2 molecules decreases $\rho(\Delta\Phi/k_BT)$ since some of the free volume is already occupied. However, although accessible sites are harder to find, they are energetically slightly more favorable as the penetrant can now interact with both the matrix and the other penetrants. This explains the small shift of the peak toward the left as P increases. Figure 7c displays some $\rho(\Delta\Phi/k_BT)$ for slabs situated in the dense part of the pure membrane. They can basically be superimposed, and their dependence on P (not shown) weakens because of the limited number of penetrants being able to penetrate as far. As noted before, the middle part of our model is more characteristic of surface chains than of true bulk chains: a slightly lower density (3%) and configurations which are aligned and flattened, even if the latter features are well attenuated. In order to assess their influence on the insertion energy density distributions, the same analysis was carried out on a 56025-atom isotropic bulk ODPA−ODA model.[23] The resulting $\rho(\Delta\Phi/k_BT)$ curve is also presented in Figure 7c. Within the statistical uncertainties, the bulk distribution is almost indistinguishable from the low-$|z|$ slabs in our dense membrane model. This supports the hypothesis that penetrant behavior is mostly dependent on very local features in the matrix, rather than on larger-scale characteristics.

Although the probability density distributions displayed in Figure 7c are skewed to the right, this region corresponds to positive $\Delta\Phi$, which actually have very small Boltzmann weights. If one considers the corresponding Boltzmann-weighted energy probability distributions, we find that they can actually all be fitted by a Gaussian, which is in agreement with the site-distribution SD model of Kirchheim.[6,7] We have to be cautious though as different approaches are being considered. The TPI method samples the insertion energy upon adding one extra particle to the system under study whereas the SD model was developed within the framework of continuum theories and experimental pressure-concentration isotherms (penetrant molecules already present in the polymer) are used to evaluate the parameters of the Gaussian energy distributions. However, these different approaches are likely to be related to the same phenomena, that is sorption in glassy polymers can indeed be related to single Gaussian distributions of site energies rather than to the two-energy-level of the dual-mode sorption model.[6]

4.4. Total Chemical Potential. An estimate of the total chemical potential resolved as a function of z, $\mu(z)$, is given by[106]

$$\mu(z) = \mu_{ig}(z) + \mu_{ex}(z) \approx -k_BT \ln\left(\frac{Vq}{n\Lambda^3}\right) - k_BT \ln\left\langle \exp\left(\frac{-\Delta U}{k_BT}\right)\right\rangle$$
$$= -k_BT\left(\ln\left(\frac{mq}{\rho_{gas}(z)\Lambda^3}\right) + \ln(p_{ip}(z))\right) \quad (6)$$

where $\mu_{ig}(z)$ is the ideal gas contribution, $\mu_{ex}(z)$ the excess chemical potential contribution (section 4.3), q the partition function for internal degrees of freedom, n the number of penetrants, m the mass of a penetrant, $\rho_{gas}(z)$ the penetrant density as a function of z and Λ is the de Broglie wavelength defined as

$$\Lambda = \left(\frac{h^2}{2\pi m k_BT}\right)^{1/2} \quad (7)$$

with h being Planck's constant. Equation 6 can be rewritten as

$$\mu(z) \approx -k_BT\left(\ln\left(\frac{mq}{\Lambda^3}\right) + \ln\left(\frac{1}{\rho_{gas}(z)}\right) + \ln(p_{ip}(z))\right)$$
$$= -k_BT\left(\lambda + \ln\left(\frac{p_{ip}(z)}{\rho_{gas}(z)}\right)\right) \quad (8)$$

where λ is just a constant. This implies that the gradient of the chemical potential in z is

$$\frac{\partial\mu(z)}{\partial z} = -k_BT\left(\frac{\partial \ln\left(\frac{p_{ip}(z)}{\rho_{gas}(z)}\right)}{\partial z}\right)$$
$$= -k_BT\left(\frac{1}{p_{ip}(z)}\frac{\partial p_{ip}(z)}{\partial z} + \frac{1}{\rho_{gas}(z)}\frac{\partial \rho_{gas}(z)}{\partial z}\right) \quad (9)$$

In permeation, the overall driving force producing a net flux of a permeant is thought to be related to the gradient in its chemical potential.[103−105] There should thus be a connection between the flux $J(z)$ as a function of z and the gradient of the chemical potential of the following form:[2]

$$J(z) = -U\rho_{gas}(z)\frac{\partial\mu(z)}{\partial z} \quad (10)$$

with U being a coefficient of proportionality. Figure 8a presents the function

$$-\ln\left(\frac{p_{ip}(z)}{\rho_{gas}(z)}\right) = \frac{\mu(z)}{k_BT} + \lambda$$

, which from eq 8 is the z-dependent part of the total chemical potential, in the case of the $P = 110$ bar system at 12000 ps. It is directly obtained from the logarithm of the ratio between the insertion probability and the corresponding gas density at z. The gradient leading to the net flux of gas into the membrane is clear to see, as too is the quasi-equilibrium ($\mu(z) \approx$ constant) in the interfacial and gas reservoir region.

In our molecular model, the flux $J(z)$ at time t is simply related to the number of O_2 molecules entering the membrane at t through an interface of cross-section A, whose position is set at z. It is similar to the uptake curve of Figure 4, except that the slope of the $n_{O_2}(t)$ vs t, that is the net flux through the interface, has to be smoothed over a very small interval around t. The derivative of

$$-\ln\left(\frac{p_{ip}(z)}{\rho_{gas}(z)}\right)$$

is the gradient in chemical potential, which can be multiplied by the gas density to give the right-hand term of eq 10.

$$\rho_{gas}(z)\frac{\partial\mu(z)}{\partial z}$$

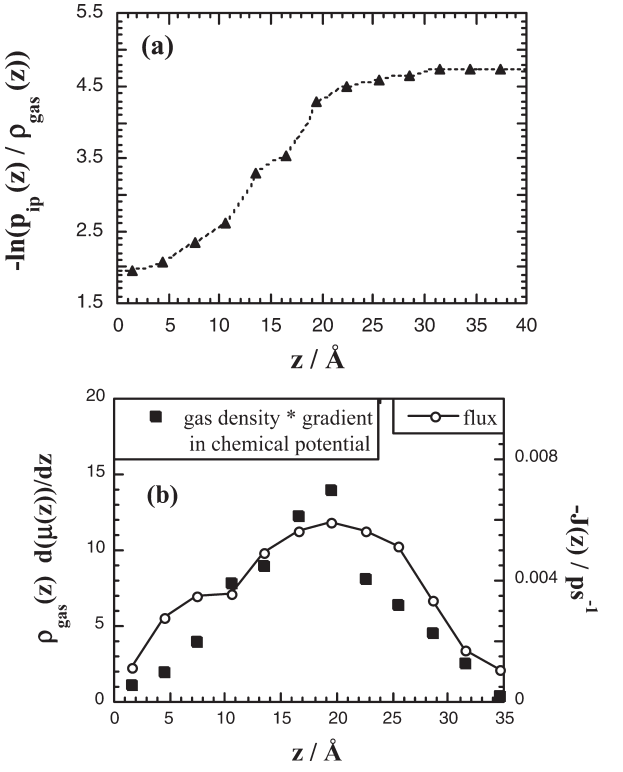

Figure 8. (a) The z-dependent part of the total chemical potential $\mu(z)$ at t = 12000 ps for the P = 110 bar system. The bin width is 3 Å. (b) Comparison between the product of the gas density times the gradient in chemical potential (black squares, arbitrary units) and the negative flux across a cross section of the MD box (circles) under the same conditions than part a.

and $-J(z)$ are compared in Figure 8b under the same conditions than Figure 8a (P = 110 bar at 12000 ps).

The raw $n_{O_2}(t)$ vs t, $p_{ip}(z)$ and $\rho_{gas}(z)$ data are all fairly noisy when taken over small time-intervals, but it is clear from Figure 8b that the correlation given in eq 10 holds well. In our model, the driving force for the movement of the penetrants is indeed directly linked to the gradient in total chemical potential.

4.5. Pressure-Dependence of the Initial Adsorption Phase. The adsorption phase was characterized by the time evolution of the z-dependent average symmetrized oxygen mass density, $\langle\rho(z)\rangle$, in the first stages of the simulations for all systems under study. Figure 9 compares the gas $\langle\rho(z)\rangle$ at 0, 1, 2, 5, 20, and 50 ps for the P = 110 bar and P = 10 bar systems.

Parts a and b of Figure 9 confirm that the penetrants reach the vicinity and even enter the dense part of the membrane within a very few picoseconds, while the evolution of the density profiles is much slower after that. The gas density curves are much smoother for P = 110 bar than for P = 10 bar for obvious statistical reasons. However, all five systems under study display exactly the same behavior. The nature of adsorption is characterized in Figure 10 where the penetrant concentrations at very short times (t = 5 ps and t = 50 ps) for L = 46 Å are displayed as a function of the reservoir pressure.

The data at very short times fit very well to a purely Langmuir form, i.e., the second part of eq 5. The heterogeneous membrane surface can thus be considered as containing a fairly constant number of adsorption sites for the penetrant. The rate of advancement in the z-direction region is of the order of ~1−2 Å ps^{-1}. This is much faster than expected from the diffusion coefficient within the dense

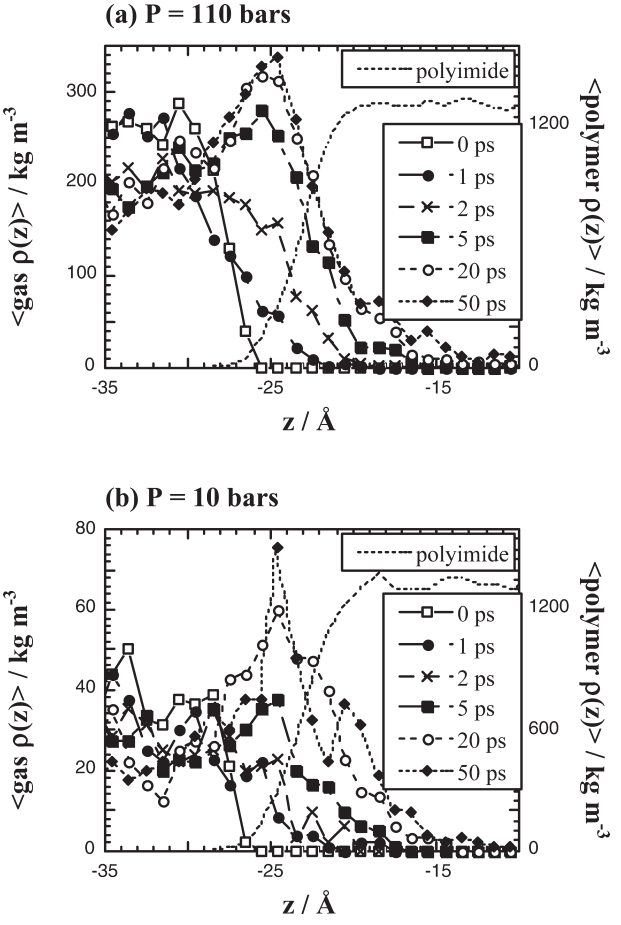

Figure 9. Left axis: time evolution of the average gas mass density distribution $\rho(z)$ at the start of the simulation run for the (a) P = 110 bar and (b) P = 10 bar systems. Right axis: the corresponding polyimide average mass density as a function of z.

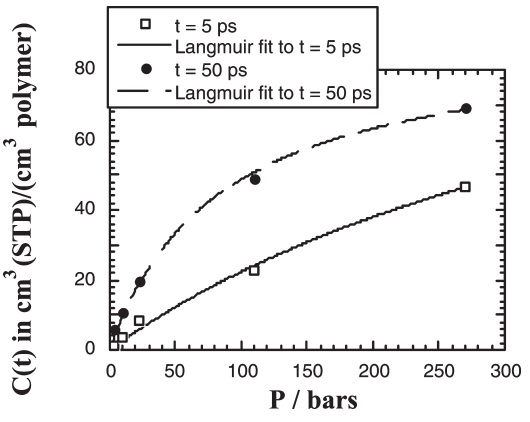

Figure 10. Average gas concentrations, $C(t)$, in the membrane with a definition for the thickness of L = 46 Å at very short simulation times as a function of reservoir pressure P. Data from the simulations are displayed as symbols. The lines are fits of the data to the Langmuir sorption isotherm model (second part of eq 5).

matrix ($D_{penetrant}$ ~0.01 Å^2 ps^{-1} for the highest pressure)[48] and is reminiscent of the gas phase behavior. From the gas MSD in the middle of the reservoirs, it is possible to estimate the gas phase diffusion coefficient D_{gas} as being ~120 Å^2 ps^{-1} for P = 4 bar, ~110 Å^2 ps^{-1} for P = 10 bar, ~100 Å^2 ps^{-1} for P = 23 bar, ~60 Å^2 ps^{-1} for P = 110 bar and ~25 Å^2 ps^{-1} for P = 270 bar. While penetrants are slowed down at the polymer interface, mobility is still closer to that of the pure

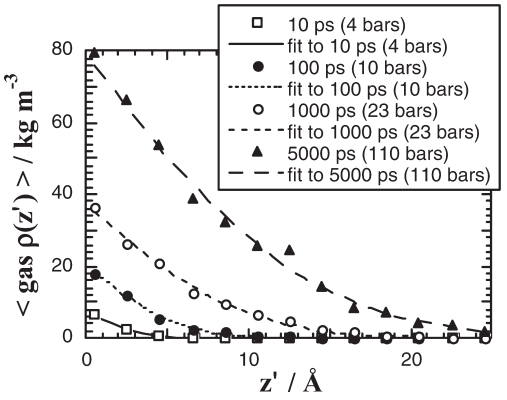

Figure 11. Mass density distributions of oxygens as a function of $z' = z + (L/2)$ in a membrane of width $L = 40$ Å averaged over specific time-intervals t. The actual profiles, displayed with symbols, come from different systems which are indicated in parentheses. The slab width is 1 Å. The lines are fits to the erfc form of eq 11.

gas phase. Even if the surface coverage remains fairly constant following the initial adsorption, the continuous exchanges of O_2 molecules between the interfaces and the gas reservoirs are also in agreement with the Langmuir model, based on gas molecules which constantly condense and evaporate at the surface.[97]

4.6. The Limiting Diffusion Phase. Once the adsorption phase is completed, the reservoirs settle into a profile which remains fairly stable over the MD simulations time scale.[48] A slower uptake mode then takes over with some O_2 penetrating into the denser part of the membrane. This is best illustrated by the uptake curve for $L = 26$ Å in Figure 4, which restricts the definition of the membrane to its middle part and does not take into account any molecules adsorbed at the vicinity of the interface. As before,[24,46−48] this slower diffusion mode can be characterized by fitting the time-dependent gas density distributions in the membrane of width L to the following solution of the one-dimensional diffusion equation in a semi-infinite system:[95,96]

$$C(z', t) = C_0 \,\mathrm{erfc}\left(\frac{z'}{\sqrt{4D_{penetrant}\,t}}\right) \qquad (11)$$

with C being the concentration of the penetrant within the medium, C_0 its concentration at the interface, $D_{penetrant}$ its diffusion coefficient in the medium, t the time-interval considered and z' the coordinate in a reference system where $z' = 0$ is the left edge of the medium which extends to $z' = +\infty$. In our models, z' is easily defined as being $z + L/2$ for the left side, but the infinite condition on the right side implies that the penetrants should not exit on the other side of the membrane. As noted in section 4.1, some O_2 molecules are able to cross the membrane in our simulations, but their relative number remains so limited ($< 0.2\%$ for $P = 270$ bar, $< 0.1\%$ for $P = 110$ bar and 0 for $P = 23, 10, 4$ bar) that they can be safely neglected here. It should also be noted that the boundary conditions associated with eq 11 are $C(z' \geq 0, t = 0) = 0$ and $C(z' = 0, t > 0) = C_0$.

For all systems under study, oxygen concentrations vs time curves were obtained by artificially labeling gas probes as being on the "left", $z_i(t_0) < -L/2$, or on the "right", $z_i(t_0) > L/2$ at any particular time origin t_0 and then following the z evolution of the distributions of these t_0-labeled atoms. All possible time origins were used and the distributions for "left" and "right" molecules were symmetrized. Such curves obtained for several time-intervals t using $L = 40$ Å in

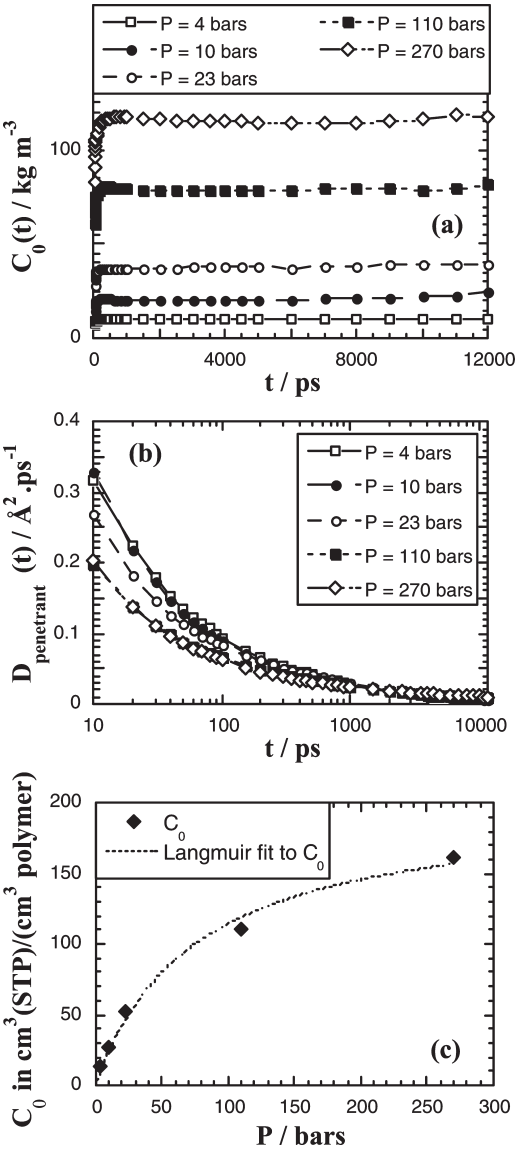

Figure 12. Time-interval t-dependence of the (a) C_0 and (b) $D_{penetrant}$ parameters used in the erfc fits (eq 11) for the mass density distributions of oxygens having entered the membrane of width $L = 40$ Å. (c) C_0 as a function of reservoir pressure P. The actual data are the black diamonds, while the line is the corresponding fit to the Langmuir sorption model (second part of eq 5).

different systems are displayed with symbols in Figure 11. The lines are the corresponding fits to eq 11 with C_0 and $D_{penetrant}$ being treated as free parameters. They show clearly that model gas density profiles are very well described with this erfc form. Even if the overall statistics get worse when P decreases and/or t increases, eq 11 fits our simulation data for all pressures under study and for all time-intervals considered.

In the boundary conditions associated with eq 11, the concentration at the interface C_0 is supposed to remain constant. In practice,[48] this condition is strongly dependent on the choice of L and the fits can lead to varying C_0 as a function of t, i.e., $C_0(t)$. If L is set well into the dense part of the membrane (e.g., $L = 26$ Å), $C_0(t)$ tends to increase with t, which is consistent with a nonequilibrium uptake at the so-called interface. On the other hand, if L is defined in the very low densities regions (e.g., $L = 46$ Å), $C_0(t)$ decreases with t, which means that the reservoir is being drained. Carrying on such analyses for various values of L showed that the "true

width" of our ODPA−ODA membrane with respect to this slower diffusion mode was obtained for $L = 40$ Å.[48] This is confirmed by Figure 12a, which shows that $C_0(t)$ as a function of t is constant for all five systems under study using that definition of L. The initial fast increase at very short times ($t < 50$ ps) is always present, regardless of L, and is certainly related to the continuous exchanges between molecules in the gas phase and molecules adsorbed at the interface. However $C_0(t)$ levels off rapidly afterward to a constant C_0 value. The corresponding $D_{penetrant}(t)$ parameters obtained from the same fits are given in Figure 12b.

The C_0 parameter, that is the concentration at the interface of the slow diffusion mode is displayed as a function of pressure P in Figure 12c and is also clearly well described by the Langmuir model. These values, shown in $cm^3(STP)/(cm^3$ polymer), are effectively an estimate of what the equilibrium concentration across our ODPA−ODA model membrane would have been if the simulation times had been long enough to attain equilibrium. This is presently too costly to attain for fully atomistic glassy polymer models of this size. On the other hand, the diffusion coefficient $D_{penetrant}(t)$, which varies with t for short time-intervals, tends toward the same value at longer t (Figure 12b). The short-time behavior is similar to that found in bulk MD simulations of glassy polymers where penetrants first display an anomalous regime with time-dependent diffusion coefficients before settling to a limiting value in the Einstein regime.[23,82] Since it occurs on such fast time scales, experimental permeation data only report the limiting value, but the presence of an anomalous regime has been proven experimentally with diffusion experiments of high concentration aqueous $CuSO_4$ into deionized water.[107] Taking into account the logarithmic scale of the x-axis in Figure 12b, the differences between the various P remain small and all curves eventually do tend toward the limiting value of $D_{penetrant} \approx 0.01$ Å^2 ps^{-1} $= 10 \times 10^{-7}$ cm^2 s^{-1}. This is about 4 times higher than that in the bulk, which has been attributed to the slightly lower-density associated with the specific configurations of the chains in the core of the membrane model.[24,47,48] However, in terms of reservoir size, the diffusion coefficient of the slower mode is clearly independent of the applied pressures P in our five models. This agrees as well with experiment, where the diffusion coefficient for light gases such as O_2 has been shown to be independent of gas concentration.[108]

5. Conclusion

Five large-scale MD simulations of oxygen transport in a ∼50000-atom fully atomistic glassy ODPA−ODA polyimide membrane model were carried out with varying sizes for the gas reservoirs. The pressures considered in these types of simulations (up to several hundred bar) usually have to be much higher than those used experimentally (∼2−3 bar for O_2), so as to have enough penetrants going into the membrane within the limited time scale available to MD simulations. The goal of this work was thus to assess whether such MD models can reproduce the experimental behavior in spite of the significantly larger pressure range, and accurately describe the transport phenomena at the polymer surfaces. The reservoir pressures were evaluated in the regions of the reservoirs where the probability of insertion of O_2 was close to 1. These pressures were consistent regardless of whether they were obtained indirectly from the gas density and the equation of state of the model pure O_2, or from measuring directly the P_{zz} pressure tensor component from the atomic momentum flux across virtual interfaces placed perpendicular to z. The five average pressures considered here were $P \approx 4$, 10, 23, 110, and 270 bar.

Because of a strong chemical potential gradient, the penetrants undergo a Langmuir-type sorption at the surface of the polymer in the very first stages of the simulations ($t < 50$ ps). The penetrant sorbs into nonequilibrium microvoids and this saturation of the interface lowers significantly the solubility of the penetrant in the interfacial region of the membrane, while a quasi-equilibrium is quickly established with the gas phase. Once the initial adsorption phase is completed, a second slower and limiting diffusion mode then takes over. It can be described by fitting an erfc solution of the one-dimensional diffusion equation in a semi-infinite system to the density of those gas molecules having entered the membrane over specific time-intervals. The parameters obtained from the fits are the concentration at the interface, which also follows the Langmuir model as a function of pressure, and the diffusion coefficient of the penetrant in the membrane, which is found to be independent of pressure.

Compared to experiment, all significant features are being reproduced in our model. Concave gas uptake vs pressure curves are obtained, the total gradient in chemical potential is found to be the driving force for permeation and no plasticizing effects are seen, even at the highest O_2 pressures. The uptake vs pressure curves can be described by the popular DMS model, but we do not find any evidence of two different populations at the molecular level. The Boltzmann weighted insertion energy probability density distributions, which are found to be Gaussian, support rather the site-distribution SD model. These simulations thus add a molecular picture to oxygen sorption in glassy polymer membranes. We intend to apply this approach to different chemical structures for the matrix and to different probes, i.e., either to penetrants similar to O_2, which do not modify the matrix much,[2,109−112] or some more soluble gases such as CO_2, which are able to lead to plasticizing effects.[113,114]

Acknowledgment. The IDRIS, CINES, and CCRT French supercomputing centres as well as the MUST Linux cluster at the University of Savoie are acknowledged for their generous provision of computer time.

References and Notes

(1) Koros, W. J.; Mahajan, R. *J. Membr. Sci.* **2000**, *175*, 181–196.
(2) Yampolskii, Y.; Pinnau, I.; Freeman, B. D. *Materials Science of Membranes*; John Wiley & Sons Ltd.: Chichester, U.K., 2006.
(3) Paul, D. R. *Ber. Bunsen-Ges.* **1979**, *83*, 294–302.
(4) Bondar, V. I.; Kamiya, Y.; Yampolskii, Y. P. *J. Polym. Sci., Part B: Polym. Phys.* **1996**, *34*, 369–378.
(5) Kanehashi, S.; Nagai, K. *J. Membr. Sci.* **2005**, *253*, 117–138.
(6) Kirchheim, R. *Macromolecules* **1992**, *25*, 6952–6960.
(7) Gotthardt, P.; Grüger, A.; Brion, H. G.; Plaetschke, R.; Kirchheim, R. *Macromolecules* **1997**, *30*, 8058–8065.
(8) Ohya, H.; Kudryavtsev, V. V.; Semenova, S. I. *Polyimide Membranes - Applications, Fabrication and Properties*; copublished by Kodansha Ltd. and Gordon and Breach Science Publishers S.A.: Tokyo and Amsterdam, 1996.
(9) Paul, D. R.; Yampolskii, Y. P. *Polymeric Gas Separation Membranes*; CRC Press: Boca Raton, FL, 1994.
(10) Ghosh, M. K.; Mittal, K. L. *Polyimides: fundamentals and applications*; Marcel Dekker, Inc.: New York, 1996.
(11) O'Brien, K. C.; Koros, W. J.; Husk, G. R. *Polym. Eng. Sci.* **1987**, *27* (3), 211–217.
(12) McHattie, J. S.; Koros, W. J.; Paul, D. R. *Polymer* **1991**, *32*, 2618.
(13) Chen, K. M.; Wang, T. H.; King, J. S. *J. Appl. Polym. Sci.* **1993**, *48*, 291–297.
(14) Mensitieri, G.; Del Nobile, M. A.; Monetta, T.; Nicodemo, L.; Bellucci, F. *J. Membr. Sci.* **1994**, *89*, 131–141.
(15) Shishatskii, A. M.; Yampolskii, Y. P.; Peinemann, K.-V. *J. Membr. Sci.* **1996**, *112*, 275–285.
(16) Kawakami, H.; Mikawa, M.; Nagaoka, S. *J. Membr. Sci.* **1996**, *118*, 223–230.
(17) Joly, C.; Le Cerf, D.; Chappey, C.; Langevin, D.; Muller, G. *Sep. Purif. Technol.* **1999**, *16*, 47–54.

(18) Pandey, P.; Chauhan, R. S. *Prog. Polym. Sci.* **2001**, *26*, 853–893.
(19) Recio, R.; Palacio, L.; Pradanos, P.; Hernandez, A.; Lozano, A. E.; Marcos, A.; De la Campa, J. G.; De Abajo, J. *J. Membr. Sci.* **2007**, *293*, 22–28.
(20) Allen, M. P.; Tildesley, D. J. *Computer Simulation of Liquids*; Clarendon Press: Oxford, England, 1987.
(21) Pinel, E.; Brown, D.; Bas, C.; Mercier, R.; Albérola, N. D.; Neyertz, S. *Macromolecules* **2002**, *35*, 10198–10209.
(22) Heuchel, M.; Hofmann, D.; Pullumbi, P. *Macromolecules* **2004**, *37*, 201–214.
(23) Neyertz, S.; Brown, D. *Macromolecules* **2004**, *37*, 10109–10122.
(24) Neyertz, S. *Soft Mater.* **2007**, *4*, 15–83.
(25) Neyertz, S. *Macromol. Theory Simul.* **2007**, *16*, 513–524.
(26) Marque, G.; Neyertz, S.; Verdu, J.; Prunier, V.; Brown, D. *Macromolecules* **2008**, *41*, 3349–3362.
(27) Neyertz, S.; Brown, D. *J. Chem. Phys.* **2001**, *115*, 708–717.
(28) Pandiyan, S.; Brown, D.; van der Vegt, N. F. A.; Neyertz, S. *J. Polym. Sci., Part B: Polym. Phys.* **2009**, *47*, 1166–1180.
(29) Natarajan, U.; Mattice, W. L. *J. Membr. Sci.* **1998**, *146*, 135–142.
(30) Clancy, T. C.; Mattice, W. L. *Comp. Theor. Polym. Sci.* **1999**, *9*, 261–270.
(31) Chang, J.; Han, J.; Yang, L.; Jaffe, R. L.; Yoon, D. Y. *J. Chem. Phys.* **2001**, *115* (6), 2831–2840.
(32) Doruker, P.; Mattice, W. L. *Macromolecules* **1998**, *31*, 1418–1426.
(33) Ayyagari, C.; Bedrov, D. *Polymer* **2004**, *45*, 4549–4558.
(34) Ijantkar, A. S.; Natarajan, U. *Polymer* **2004**, *45*, 1373–1381.
(35) Prathab, B.; Aminabhavi, T. M.; Parthasarathi, R.; Manikandan, P.; Subramanian, V. *Polymer* **2006**, *47*, 6914–6924.
(36) Clancy, T. C.; Jang, J. H.; Dhinojwala, A.; Mattice, W. L. *J. Phys. Chem. B* **2001**, *105*, 11493–11497.
(37) Jang, J. H.; Mattice, W. L. *Polymer* **1999**, *40*, 1911–1914.
(38) Eilhard, J.; Zirkel, A.; Tschöp, W.; Hahn, O.; Kremer, K.; Schärpf, O.; Richter, D.; Buchenau, U. *J. Chem. Phys.* **1999**, *110*, 1819–1830.
(39) Queyroy, S. Ph.D. Thesis, University of Savoie: Le Bourget du Lac, France, **2004**.
(40) Queyroy, S.; Neyertz, S.; Brown, D.; Müller-Plathe, F. *Macromolecules* **2004**, *37* (19), 7338–7350.
(41) Harmandaris, V. A.; Adhikari, N. P.; Van der Vegt, N. F. A.; Kremer, K. *Macromolecules* **2006**, *39*, 6708–6719.
(42) Hess, B.; León, S.; Van der Vegt, N.; Kremer, K. *Soft Matter* **2006**, *2*, 409–414.
(43) Harmandaris, V. A.; Reith, D.; Van der Vegt, N. F.; Kremer, K. *Macromol. Chem. Phys.* **2007**, *208*, 2109–2120.
(44) Smit, E.; Mulder, M. H. V.; Smolders, C. A.; Karrenbeld, H.; Van Eerden, J.; Feil, D. *J. Membr. Sci.* **1992**, *73* (2−3), 247–257.
(45) Zhang, R.; Mattice, W. L. *J. Membr. Sci.* **1995**, *108*, 15–23.
(46) Neyertz, S.; Douanne, A.; Brown, D. *Macromolecules* **2005**, *38*, 10286–10298.
(47) Neyertz, S.; Douanne, A.; Brown, D. *J. Membr. Sci.* **2006**, *280*, 517–529.
(48) Neyertz, S.; Brown, D. *Macromolecules* **2008**, *41*, 2711–2721.
(49) Bas, C.; Mercier, R.; Sanchez-Marcano, J.; Neyertz, S.; Albérola, N. D.; Pinel, E. *J. Polym. Sci., Part B: Polym. Phys.* **2005**, *43*, 2413–2426.
(50) Brown, D. *The gmq User Manual Version 4*: available at http://www.lmops.univ-savoie.fr/brown/gmq.html, **2008**.
(51) Ewald, P. P. *Ann. Phys.* **1921**, *64*, 253–287.
(52) Smith, W. *Comput. Phys. Commun.* **1992**, *67*, 392.
(53) Pinel, E.; Mercier, R.; Sanchez-Marcano, J. G.; Neyertz, S.; Albérola, N. D.; Bas, C. *C. R. Chim.* **2003**, *6*, 493–499.
(54) Pinel, E. Ph. D. Thesis, University of Savoie: Le Bourget du Lac, France, **2001**.
(55) Kikuchi, H.; Kuwajima, S.; Fukuda, M. *J. Chem. Phys.* **2001**, *115*, 6258–6265.
(56) Kikuchi, H.; Kuwajima, S.; Fukuda, M. *Chem. Phys. Lett.* **2002**, *358*, 466–472.
(57) Berendsen, H. J. C.; Postma, J. P. M.; Van Gunsteren, W. F.; DiNola, A.; Haak, J. R. *J. Chem. Phys.* **1984**, *81*, 3684–3690.
(58) Tsige, M.; Grest, G. S. *Macromolecules* **2004**, *37*, 4333–4335.
(59) Tsige, M.; Mattsson, T. R.; Grest, G. S. *Macromolecules* **2004**, *37*, 9132–9138.
(60) Mansfield, K. F.; Theodorou, D. N. *Macromolecules* **1990**, *23*, 4430–4445.
(61) Mansfield, K. F.; Theodorou, D. N. *Macromolecules* **1991**, *24*, 6283–6294.
(62) Jang, J. H.; Mattice, W. L. *Polymer* **1999**, *40*, 4685–4694.
(63) Jang, J. H.; Ozisik, R.; Mattice, W. L. *Macromolecules* **2000**, *33*, 7663–7671.
(64) Doruker, P.; Mattice, W. L. *Macromol. Theory Simul.* **2001**, *10*, 363–367.
(65) Jain, T. S.; De Pablo, J. J. *Macromolecules* **2002**, *35*, 2167–2176.
(66) Xu, G.; Mattice, W. L. *J. Chem. Phys.* **2003**, *118*, 5241–5247.
(67) Kikuchi, H.; Fukura, M. *KGK Kautsch. Gummi Kunstst.* **2004**, *57*, 416–422.
(68) Baljon, A. R. C.; Van Weert, M. H. M.; Barber DeGraaff, R.; Khare, R. *Macromolecules* **2005**, *38*, 2391–2399.
(69) Ochoa, J. G. D.; Binder, K.; Paul, W. *J. Phys.: Condens. Matter* **2006**, *18*, 2777–2787.
(70) Peter, S.; Meyer, H.; Baschnagel, J. *J. Polym. Sci., Part B: Polym. Phys.* **2006**, *44*, 2951–2967.
(71) Morita, H.; Tanaka, K.; Kajiyama, T.; Nishi, T.; Doi, M. *Macromolecules* **2006**, *39* (18), 6233–6237.
(72) Helfand, E.; Tagami, Y. *J. Chem. Phys.* **1972**, *56*, 3592–3601.
(73) Helfand, E.; Tagami, Y. *J. Chem. Phys.* **1972**, *57*, 1812–1813.
(74) Ten Brinke, G.; Ausserre, D.; Hadziioannou, G. *J. Chem. Phys.* **1988**, *89*, 4374–4380.
(75) Bitsanis, I.; Hadziioannou, G. *J. Chem. Phys.* **1990**, *92*, 3827–3847.
(76) Vacatello, M. *Macromol. Theory Simul.* **2001**, *10*, 187–195.
(77) Vacatello, M. *Macromol. Theory Simul.* **2002**, *11*, 53–57.
(78) Mischler, C.; Baschnagel, J.; Binder, K. *Adv. Colloid Interface Sci.* **2001**, *94*, 197–227.
(79) Izumisawa, S.; Jhon, M. S. *J. Chem. Phys.* **2002**, *117*, 3972–3977.
(80) Fisher, J.; Lago, S. *J. Chem. Phys.* **1983**, *78*, 5750–5758.
(81) Widom, B. *J. Chem. Phys.* **1963**, *39*, 2808–2812.
(82) Müller-Plathe, F. *Acta Polym.* **1994**, *45*, 259–293.
(83) Haile, J. M. *Molecular Dynamics Simulation: Elementary Methods*; Wiley: New York, 1992.
(84) Tanaka, K.; Okano, M.; Toshino, H.; Kita, H.; Okamoto, K.-I. *J. Polym. Sci., Part B: Polym. Phys.* **1992**, *30*, 907–914.
(85) Yamamoto, H.; Horii, F.; Odani, H. *Macromolecules* **1989**, *22*, 4130.
(86) Stern, S. A.; Mi, Y.; Yamamoto, H. *J. Polym. Sci., Part B: Polym. Phys.* **1989**, *27*, 1887–1909.
(87) Li, Y.; Wang, X.; Ding, M.; Xu, J. *J. Appl. Polym. Sci.* **1996**, *61*, 741–748.
(88) Kim, T. H.; Koros, W. J.; Husk, G. R.; O'Brien, K. C. *J. Membr. Sci.* **1988**, *37*, 45–62.
(89) Stern, S. A.; Liu, Y.; Feld, W. A. *J. Polym. Sci., Part B: Polym. Phys.* **1993**, *31*, 939–951.
(90) Humphrey, W.; Dalke, A.; Schulten, K. *J. Mol. Graphics* **1996**, *14* (1), 33–38.
(91) Gusev, A. A.; Müller-Plathe, F.; van Gunsteren, W. F.; Suter, U. W. *Adv. Polym. Sci.* **1994**, *116*, 207–247.
(92) Gusev, A. A.; Suter, U. W.; Moll, D. J. *Macromolecules* **1995**, *28*, 2582–2584.
(93) Hiltner, A.; Liu, R. Y. F.; Hu, Y. S.; Baer, E. *J. Polym. Sci., Part B: Polym. Phys.* **2005**, *43*, 1047–1063.
(94) Barbier, D.; Brown, D.; Grillet, A.-C.; Neyertz, S. *Macromolecules* **2004**, *37* (12), 4695–4710.
(95) Crank, J. C. *The Mathematics of Diffusion*, 2nd ed.; Oxford University Press: Oxford, U.K., 1979.
(96) Tsige, M.; Grest, G. S. *J. Chem. Phys.* **2004**, *120*, 2989–2995.
(97) Moore, W. J. *Physical Chemistry*, 5th ed.; Prentice-Hall Inc.: Englewood Cliffs, NJ, 1972.
(98) Tokarev, A.; Friess, K.; Machkova, J.; Sipek, M.; Yampolskii, Y. P. *J. Polym. Sci., Part B: Polym. Phys.* **2000**, *44*, 832–844.
(99) Paul, D. R.; Koros, W. J. *J. Polym. Sci., Polym. Phys. Ed.* **1976**, *14*, 675–685.
(100) Sanchez, I. C.; Lacombe, R. H. *Macromolecules* **1978**, *11*, 1145–1156.
(101) De Angelis, M. G.; Merkel, T. C.; Bondar, V. I.; Freeman, B. D.; Doghieri, F.; Sarti, G. C. *J. Polym. Sci., Polym. Phys. Ed.* **1999**, *37*, 3011–3026.
(102) De Angelis, M. G.; Merkel, T. C.; Bondar, V. I.; Freeman, B. D.; Doghieri, F.; Sarti, G. C. *Macromolecules* **2002**, *35*, 1276–1288.
(103) Krishna, R.; Wesselingh, J. A. *Chem. Eng. Sci.* **1997**, *52*, 861–911.
(104) Thompson, A. P.; Ford, D. M.; Heffelfinger, G. S. *J. Chem. Phys.* **1998**, *109*, 6406–6414.
(105) Thompson, A. P.; Heffelfinger, G. S. *J. Chem. Phys.* **1999**, *110*, 10693–10705.
(106) Ben-Naim, A. *Molecular theory of solutions*; Oxford University Press: Oxford, U.K., 2006.

(107) Küntz, M.; Lavallée, P. *J. Phys. D: Appl. Phys.* **2004**, *37*, L5–L8.
(108) Alentiev, A. Y.; Shantarovich, V. P.; Merkel, T. C.; Bondar, V. I.; Freeman, B. D.; Yampolskii, Y. P. *Macromolecules* **2002**, *35*, 9513–9522.
(109) Yamamoto, H.; Mi, Y.; Stern, S. A.; St-Clair, A. K. *J. Polym. Sci., Part B: Polym. Phys.* **1990**, *28*, 2291–2304.
(110) Jia, L.; Xu, J. *Polym. J.* **1991**, *23*, 417–425.
(111) Stern, S. A. *J. Membr. Sci.* **1994**, *94*, 1–65.
(112) Li, Y.; Ding, M.; Xu, J. *Macromol. Chem. Phys.* **1997**, *198*, 2769–2778.
(113) Lin, H.; Wagner, E. V.; Freeman, B. D.; Toy, L. G.; Gupta, R. P. *Science* **2006**, *311*, 639–642.
(114) Bos, A.; Pünt, I. G. M.; Wessling, M.; Strathmann, H. *J. Membr. Sci.* **1999**, *155*, 67–78.